Korean J. Chem. Eng., **29**(7), 855-861 (2012)
DOI: 10.1007/s11814-011-0250-y

Modeling the oxidative coupling of methane using artificial neural network and optimizing of its operational conditions using genetic algorithm

Mohammad Reza Ehsani†, Hamed Bateni, and Ghazal Razi Parchikolaei

Department of Chemical Engineering, Isfahan University of Technology, Isfahan 84156-83111, Iran
(*Received 3 May 2011 • accepted 24 September 2011*)

Abstract−The effect of some operating conditions such as temperature, gas hourly space velocity (GHSV), CH_4/O_2 ratio and diluents gas (mol% N_2) on ethylene production by oxidative coupling of methane (OCM) in a fixed bed reactor at atmospheric pressure was studied over $Mn/Na_2WO_4/SiO_2$ catalyst. Based on the properties of neural networks, an artificial neural network was used for model developing from experimental data. To prevent network complexity and effective data input to the network, principal component analysis method was used and the number of output parameters was reduced from 4 to 2. A feed-forward back-propagation network was used for simulating the relations between process operating conditions and those aspects of catalytic performance including conversion of methane, C_2 products selectivity, C2 yielding and C_2H_4/C_2H_6 ratio. Levenberg-Marquardt method is presented to train the network. For the first output, an optimum network with 4-9-1 topology and for the second output, an optimum network with 4-6-1 topology was prepared. After simulating the process as well as using ANNs, the operating conditions were optimized and a genetic algorithm based on maximum yield of C_2 was used. The average error in comparing the experimental and simulated values for methane conversion, C_2 products selectivity, yield of C_2 and C_2H_4/C_2H_6 ratio, was estimated as 2.73%, 10.66%, 5.48% and 10.28%, respectively.

Key words: Oxidative Coupling of Methane (OCM), $Mn/Na_2WO_4/SiO_2$ Catalyst, ANN, Optimization, Genetic Algorithm

INTRODUCTION

1. Oxidative Coupling of Methane (OCM) Process

The very large available reserves of methane, often found in remote regions, can serve as a feedstock for chemical productions and as a source of energy in the 21st century. Although methane has currently some important applications such as heating houses and supplying the necessary hydrogen for ammonia synthesis, its potential ability for producing ethylene or liquid hydrocarbon fuels has not been fully realized [1]. As the vital building block in producing valuable chemicals, ethylene has a diverse market all over the world, and there are indications of increasing demand over the last few years. Conventionally, ethylene is produced from either naphtha steam cracking or ethane thermal cracking. However, the rising price of the feedstock induced by the global oil demand suggests that there is a need to seek for other alternatives [2].

Oxidative coupling of methane (OCM) is one of the promising routes for direct conversion of natural gas to higher hydrocarbons, especially ethylene that can be used to produce the petrochemicals or fuels. The key to OCM commercial success is identifying a suitable catalyst with capability of high C_2 selectivity at significant level of methane conversion, especially at low temperature conditions [3]. With the aim of improving ethane and ethylene's yield, there have been many researches focused on the used catalysts in OCM process, their properties and also the influential factors on their performance [4]. Fang et al. have identified $Mn/Na_2WO_4/SiO_2$ as a promising OCM catalyst. Malekzade et al. represented that the performance of $MO_x/Na_2WO_4/SiO_2$ catalysts for the oxidative coupling of methane is well correlated with the electrical conductivity of the catalysts under OCM conditions [5]. Mahmoodi and co-workers have indicated that Sodium salts and different oxo anions largely influence the structures, reducibility, and catalytic performances of the M-Na-Mn/SiO_2-based nanocatalysts (M=V, Cr, Nb, W, Mo) in the oxidative coupling of methane reaction. Among these synthesized nanocatalysts, Na_2WO_4-Mn/SiO_2 as well as Na_2MoO_4-Mn/SiO_2 shows the best catalytic performance at OCM reaction conditions [6]. In this study, $Mn/Na_2WO_4/SiO_2$ catalyst has been selected for OCM reaction because of its high catalytic performance.

2. Artificial Neural Networks

Artificial neural networks (ANNs) were inspired by biological neural networks [7,8]. ANNs are made of a large number of simple computing elements called nodes or neurons; they are arranged to form an input layer, one or more hidden layers and an output layer [9]. They mostly include the interconnections between the successive layers nodes through the so-called weights [10]. The role of these weights is to modify the signal carried from one node to the other and enhance or diminish the influence of the specific connection [9]. Each neuron in the hidden layer receives weighted inputs from each neuron in the previous layer plus one bias, as given by Eq. (1).

$$Z_i = \left(\sum_{k=1}^{N_{j-1}} X_k^{j-1} W_{k,i} + b_i \right) \tag{1}$$

where X_k^{j-1} denotes the input from k-th node in the j-th layer, $W_{k,j}$ is the weight of the link between node k and all the nodes in the previous layers, and b_i is the bias to the node, N_{j-1} is the number of

†To whom correspondence should be addressed.
E-mail: ehsanimr@cc.iut.ac.ir

nodes in the layer j−1. This sum is passed along an activation function, to produce the output of the node, calculation as $Y_i=f(Z_i)$ [8]. An activation or transfer function can be any type of mathematical function, but a sigmoid function (Eq. (2)) is the most commonly used [7,8]:

$$f(Z_i)=\frac{1}{1+e^{-Z_i}} \tag{2}$$

The internal weights of the network are adjusted in the course of an iterative process termed training [10] and the algorithm used for this purpose, the so-called training algorithm. The error back-propagation (BP) algorithm is the most common form of learning, utilized today in artificial neural networks. There are many network architectures existing, e.g., multilayer perceptron, radial basis function, probabilistic neural networks and several more types. Among them, the multilayer perceptron is the most popular [8].

For NN training, the available data are divided into three parts: training set, test set and validation set. The parameters $W_{k,i}$ and b_i are calculated from the training set. Training is continued whenever any error on the validation set starts to increase. Test set is used to evaluate neural network performance [11].

ANNs have been used for many chemical engineering applications such as steady state and dynamic process modeling, process identification, yield maximization, nonlinear control and fault detection and diagnosis [12].

3. Principal Component Analysis

Principal component analysis (PCA) is a classical data analysis method that provides a sequence of the best linear approximations to a given high-dimensional data set. It is one of the most popular techniques for dimensionality reduction [13]. There are different ways to select a subset (consisting of m principal components) from the main set variables including scree graph and cumulative percentage of total variation that, in both ways, covariance matrix, its eigenvalues and eigenvectors, must be calculated. The rule for choosing m (the number of principal components) is to select a cumulative percentage of the total variation to which it is desired to contribute the selected principal components (PCs) (for example 80% or 90%). The required number of PCs is then the smallest value of m for which this chosen percentage is exceeded. The obvious definition of percentage of variation accounted for the first m PCs is as follows:

$$t_m=100\sum_{k=1}^{m}\lambda_k\Big/\sum_{k=1}^{p}\lambda_k \tag{4}$$

Where λ_k denotes the eigenvalue (variance) of the k-th PC.

Choosing a cut-off t^* somewhere between 70% and 90% and retaining m PCs, where m is the smallest integer for which $t_m>t^*$, provides a rule which in practice preserves in the first m PCs most of the information [14].

The scree graph, which was suggested by Cattell (1966) but which was already in common use, is even more subjective in its usual form, as it involves looking at a plot of eigenvalues (λ_k) against the number of components (k) the slope of lines joining the plotted points are steep to the left of k, and not steep to the right. This value of k is then taken to be the number of components m to be retained [14,15].

All steps for the PCA method are presented as follows:

Step 1: $D_{[n\times 4]}$=Output data matrix, n: Number of experimental sample
Step 2: $D_{[n\times 4]}$=Matrix of D normalized between (0, 1)
Step 3: $D_{[n\times 4]}=D_{[n\times 4]}-$Mean (matrix of D centralized)
Step 4: Covariance matrix calculated (Cov(D))
Step 5: Calculate the cut point (m) using scree plot and cumulative proportion
Step 6: Calculate the new eigenvectors matrix
Step 7: Principal component of D=D×W, W: new eigenvectors matrix

4. Genetic Algorithm

The origin of genetic algorithms (GA) dates back in 1975 in the pioneering work of Holland [16]. GA is a stochastic and heuristic solution search or optimization technique which has been derived based on the Darwin's theory of survival of the fittest [17,18]. Each GA operates on a population of artificial chromosomes. Each chromosome represents a solution to a problem and has a fitness value [17] and these values are evaluated using a fitness function [19]. GAs normally consist of three important operators: selection, crossover and mutation. There are numerous operator types described in the literature, depending on the problem to be solved and the coding used to represent the configurations [20]. The selection operator determines which parent chromosomes participate in producing offspring of the next generation. Members with higher fitness values are more likely to be selected as the parents of a solution in the next generation. The crossover operator tries to combine the best features from different design solutions. The last commonly applied operator is mutation, used to produce variations in the population. It can be performed either during selection or crossover [21]. Genetic algorithms have many advantages over the traditional optimization methods. In particular, GAs are able to deal with discrete optimum design problems, do not need derivatives of objective functions and have the capability of identifying global optimal values of the objective function [22]. One more advantage is their generality. After appropriate problem encoding, virtually any synthesis problem can be solved with a GA [23]. The probabilistic nature of GA helps to avoid convergence to false optima. One of the major disadvantages of genetic algorithm techniques, despite having some good initial characteristics like global optimization techniques, is that they may slow down the region of identified optimal solutions considerably once [18]. It is worth noting that by combining the GA method with neural network, the advantages of both methods are exploited to produce a hybrid optimization method which is both robust and fast [18].

Among all modeling methods, although ANN is a more acceptable and accurate model, GA is able to determine the optimized operating parameters of the process. For these reasons, it is our purpose to develop a model using ANN for the fixed bed reactor at atmospheric pressure which is used for OCM reaction. In addition, GA algorithm has been applied to optimize operating conditions, based on maximum yield of C_2. Finally, the obtained model has been validated at optimum operating conditions.

EXPERIMENTAL

1. Catalyst Preparation

The $Mn/Na_2WO_4/SiO_2$ catalyst was prepared by incipient wetness impregnation method. The synthesis of catalyst was carried out by impregnating of silica support with aqueous solutions con-

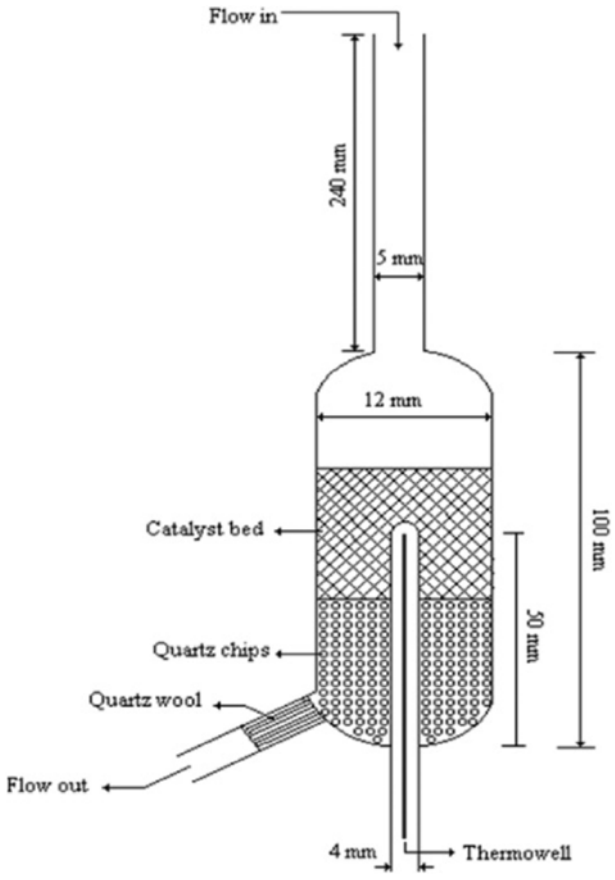

Fig. 1. Schematic drawing of reactor.

taining 2 wt% Manganese nitrate and 5 wt% sodium tungstate. Then mixture was evaporated to dryness by using vacuum and the sample was calcinated at 850 °C. The catalyst was then palletized, crushed and sieved to 20-25 mesh.

2. Reactor System

The catalytic reaction was carried out in a tubular fixed bed quartz micro reactor with internal diameter 12 mm shown in Fig. 1. The amount of 0.5 g catalyst was loaded in the quartz reactor filled with quartz granules in the test space of the reactor so far to minimize the contribution from any gas-phase reactions. The remaining space of the reactor below the catalyst bed was filled with quartz wool.

Table 1. Operating parameter and their ranges

Parameters	Range
Temperature	750-850 °C
Gas hourly space velocity (GHSV)	12,000-24,000 $cm^3g^{-1}h^{-1}$
Mol percent of N_2	20-60
Ratio of CH_4/O_2	2-6

The reactor was heated by an electrical furnace and the reaction temperature was measured with a K-type thermocouple placed in a well in the catalyst bed and controlled with T.I.C (Jumo Dicon 5.1) as well as mass flow controlled with electrical controller (Brooks 5580). Reactant gases included CH_4 (99.996%), O_2 (99.99%) and N_2 (99.99% purity). Reaction was done at different conditions but in constant atmospheric pressure. The operating parameters and their ranges are shown in Table 1. The reaction products were then analyzed with on-line gas chromatography (Chrompack) equipped with FID with helium for compounds identifying except methane and TCD for methane, using a Porapak Q column for separating ethane, ethylene and carbon monoxide and a molecular sieve column for separating oxygen, nitrogen, methane and carbon monoxide (Fig. 2). Results obtained from the products analysis represented some aspects of catalytic performance including methane conversion, C_2 products selectivity, and yield of C_2 and C_2H_4/C_2H_6 ratio.

Some of the important parameters are defined as:

$$\text{Methane conversion: } x_{CH_4}(\%) = \frac{\text{moles of } CH_4 \text{ converted}}{\text{moles of } CH_4 \text{ in feed}} \times 100$$

Selectivity of C_2 product:

$$S_{C_2}(\%) = \frac{\sum(2 \times \text{moles of } C_2)}{\text{moles of } CH_4 \text{ converted to all products}}$$

Yield of C_2 product: $Y_{C_2}(\%)$=Methane conversion×C_2 selectivity

$$\text{Gas hourly space velocity: } GHSV = \frac{\text{feed flow rate}}{\text{catalyst weight}} \ (cm^2g^{-1}h^{-1})$$

MODELING AND OPTIMIZING

In the present work, the effect of operating conditions such as temperature, gas hourly space velocity (GHSV), CH_4/O_2 ratio and diluents gas (mol% N_2) on ethylene production by oxidative coupling of methane (OCM) in a fixed bed reactor at atmospheric pres-

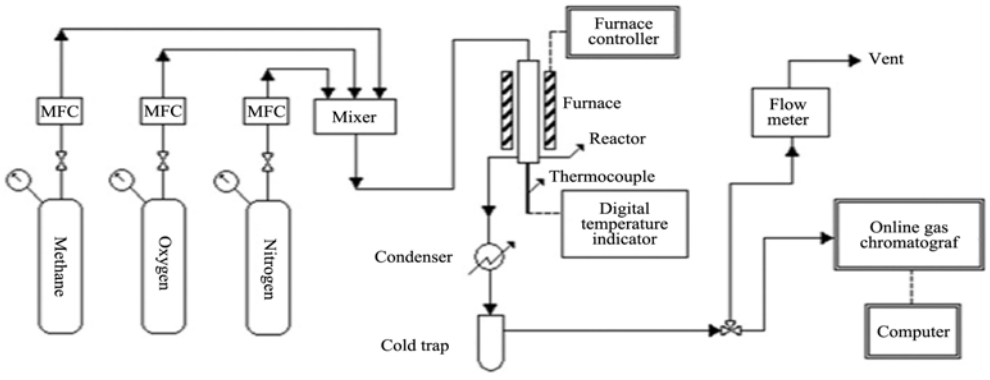

Fig. 2. Schematic diagram of experimental test rig system.

sure was studied over $Mn/Na_2WO_4/SiO_2$ catalyst and using the neural networks. The acquired data from the reactor test were used for modeling the OCM process.

The data must be pre-processed, so that the ANN becomes able to learn from it effectively. The data were analyzed statically and all the values that appeared to be scattered far away from the majority of values were considered as outliers and were excluded from the data set. After removing the desultory data between the results of 146 reactor tests, there were 100 items supposed as the database dividing in three subsets as follows: the first subset of 60 existing patterns was used to train the model, as previously discussed, the second subset of 20 patterns was the validation set used to determine when to stop the training stage, and the third data set of 20 patterns was used to test the ANN and evaluate the efficiency of ANN predictions. All of the data sets were mutually exclusive sets of vectors selected from the same measured data in the reactor tests.

A feed-forward back-propagation network, widely known as multilayer perceptron (MLP), was used for simulating the relations between process operating conditions (the above-mentioned parameters) and aspects of catalytic performance including methane conversion, C_2 products selectivity, yield of C_2 and C_2H_4/C_2H_6 ratio. To prevent network complexity, principal component analysis (PCA) method was used. In this paper, both route of cumulative percentage of total variation and scree graph have been used to determine the principal components. Cumulative percentage of total variation has been considered as 90%. The scree graph for our experiment is presented in Fig. 3. Also, values of cumulative percentage of total variations have been reported in this figure.

Covariance matrix, the eigenvalues and eigenvectors of covariance matrix has been obtained as follows:

$$\mathrm{Cov(D)}=\begin{bmatrix} 0.0602 & 0.0034 & 0.0588 & 0.0382 \\ 0.0034 & 0.0375 & 0.0254 & 0.0114 \\ 0.0588 & 0.0254 & 0.0739 & 0.0447 \\ 0.0382 & 0.0114 & 0.0447 & 0.0372 \end{bmatrix}$$

$$\mathrm{Eigenvalues}=\begin{bmatrix} 0.00147 & 0 & 0 & 0 \\ 0 & 0.0079 & 0 & 0 \\ 0 & 0 & 0.0391 & 0 \\ 0 & 0 & 0 & 0.1603 \end{bmatrix}$$

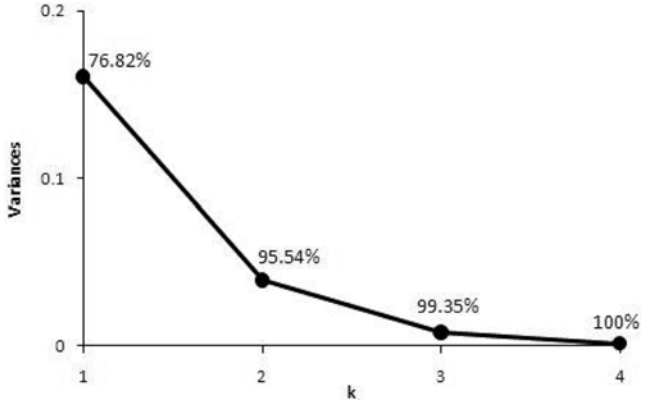

Fig. 3. Scree graph for output data (value on the diagram denote the cumulative percentage).

$$\mathrm{Eigenvevtors}=\begin{bmatrix} 0.0618 & 0.3489 & -0.4268 & 0.5673 \\ 0.3997 & 0.0743 & 0.8926 & 0.1947 \\ -0.6791 & 0.2674 & 0.1357 & 0.6700 \\ 0.0688 & -0.8951 & -0.0517 & 0.4375 \end{bmatrix}$$

According to Fig. 3, the first two variables have been chosen as the principal components by preserve 95.54% of variation (m=2). Therefore, by multiplying the output data matrix (D) in the third and fourth column of the eigenvectors matrix (W), a new matrix consisting of two columns was obtained (New D), and dimensions of data and subsequently the numbers of neural network output were reduced from 4 to 2.

$$\mathrm{NewD}=\mathrm{D}\times\mathrm{W}$$

$$\mathrm{W}=\begin{bmatrix} -0.4268 & 0.5673 \\ 0.8926 & 0.1947 \\ 0.1357 & 0.6700 \\ -0.0517 & 0.4375 \end{bmatrix}$$

Then, the initial ANN structure consisted of 4 and 2 nodes in input and output layer, respectively (shown in Fig. 4).

Because of independent operation of each 2 nodes available at output layer and in order to avoid network complexity, there were two specific neural networks designed for each output as shown in Fig. 5 (network_out1 for out1 and network_out2 for out2). Levenberg-Marquardt method was presented to train the networks. The tangent-sigmoid function (Eq. (3)) was used as the activation function in both the hidden and the output layers.

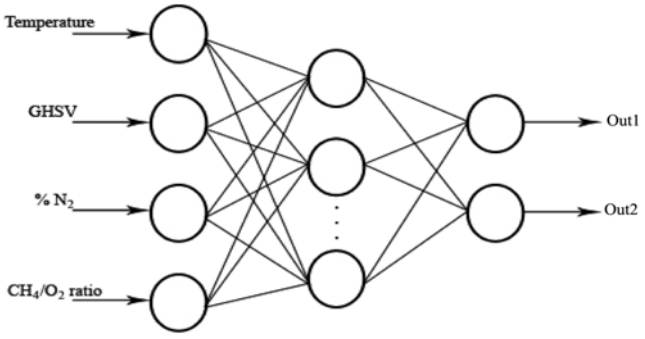

Fig. 4. Initial ANN structure.

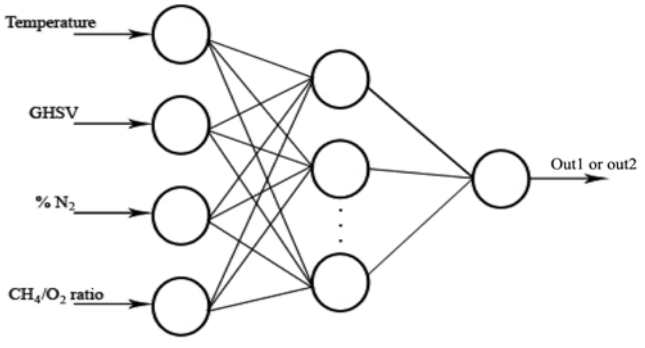

Fig. 5. Final structure of networks.

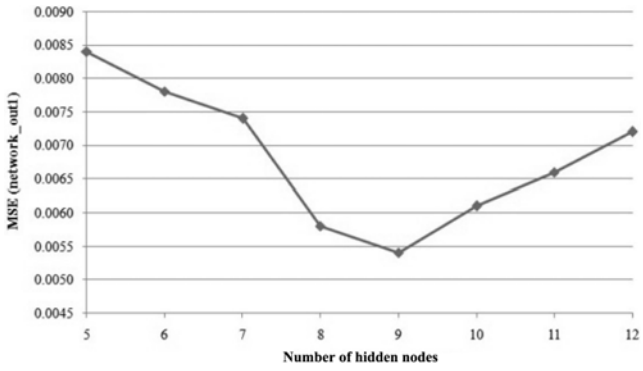

Fig. 6. Plot showing the dependence of the MSE for the test data set on the number of hidden nodes in network_out1.

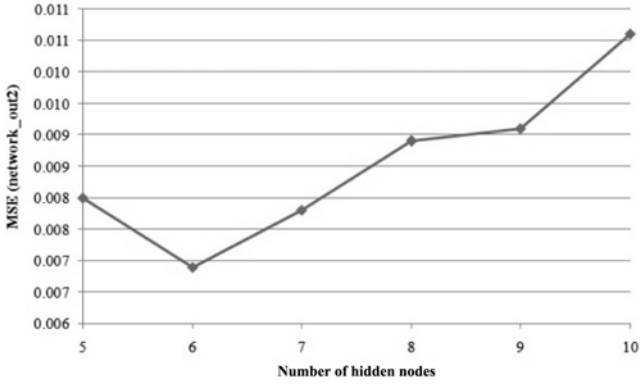

Fig. 7. Plot showing the dependence of the MSE for the test data set on the number of hidden nodes in network_out2.

$$\text{tansig}(n) = \frac{e^{n} - e^{-n}}{e^{n} + e^{-n}} \quad (3)$$

For supplementing ANN structure, the number of nodes in hidden layer must be determined and the number of optimum nodes was selected based on minimum mean squared error (MSE) on the test data set.

MSE (energy function) of different NN models for Network_out1 and Network_out2, against the number of neurons in the hidden layer are, respectively, plotted (shown in Figs. 6 and 7).

According to the aforesaid figures for the first output and the second output, there was an optimum network with 4-9-1 topology (one hidden layer which includes 9 neurons) and 4-6-1 topology (one hidden layer including 6 neurons) prepared, respectively. The obtained topologies for both neural networks must be evaluated. For this purpose, the predicted values of network_out1 (neural networks output when test data set was used as input to the networks) for different time of measurement were plotted against the experimentally measured values for the corresponding times of measurement (acquired data) as shown in Fig. 8. The calculated correlation coefficient for this network was also 0.977. Besides, there was the same work applied for network_out2, and the neural network output (predicted values) for this network was observed to fit well with the experimental data. This is also illustrated in Fig. 9. The fit was observed to be linear with correlation coefficient of 0.972.

After the simulation process using ANNs, operating conditions

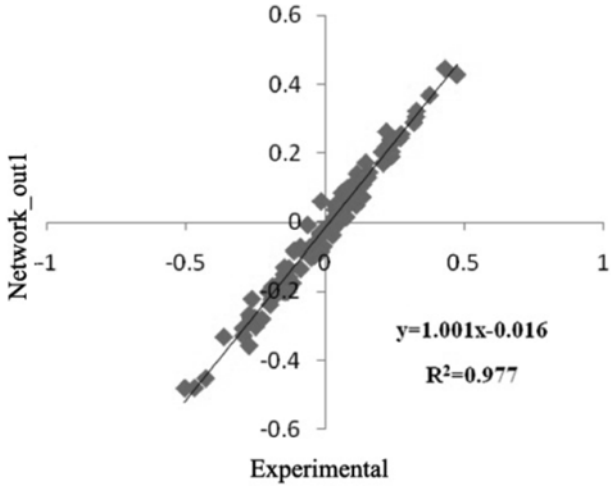

Fig. 8. Comparison of actual and ANN predicted output1 for Network_out1.

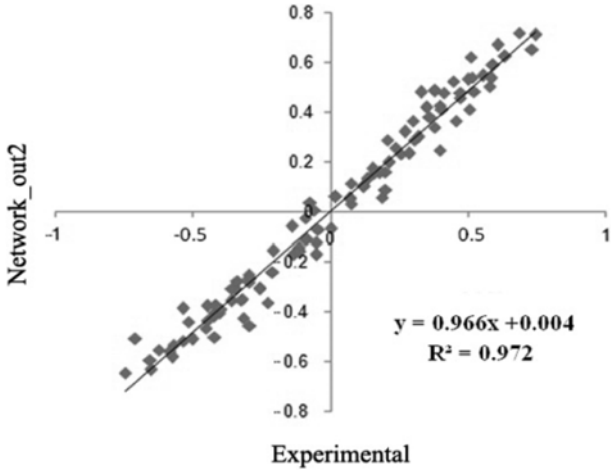

Fig. 9. Comparison of actual and ANN predicted output2 for Network_out2.

were optimized using genetic algorithm based on maximum yield of C_2. The optimum conditions were obtained as reaction temperature=850 °C, GHSV=22464 $cm^3g^{-1}h^{-1}$, diluents gas=30 (mol%) and CH_4/O_2 ratio=4 and under these optimum conditions 33% of methane conversion, 71.07% of C_2 product selectivity, 23.47% of C_2 yield and 2.073 of C_2H_4/C_2H_6 ratio were obtained. Experimental runs under optimum conditions and the obtained results were compared with the simulated values obtained from the model. The average error in comparing the experimental and simulated values for methane conversion, C_2 products selectivity, yield of C_2 and C_2H_4/C_2H_6 ratio, was estimated as 2.73%, 10.66%, 5.48% and 10.28%, respectively.

RESULTS AND DISCUSSION

In this section, ANN model was used to investigate the effect of operation conditions on OCM process.

In all of the following figures, just one of the parameters was changed in the specified range mentioned in Table 1, whereas other parameters were fixed according to the specified optimum condi-

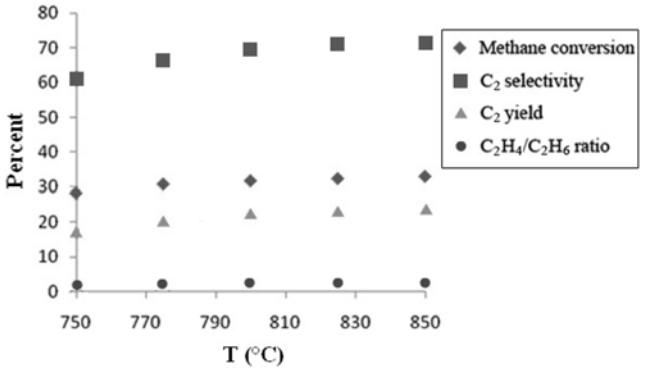

Fig. 10. Temperature profile of OCM reaction on $Mn/Na_2WO_4/SiO_2$ catalyst with CH_4/O_2 ratio=4, GHSV=22,464 $cm^3g^{-1}h^{-1}$, mol% N_2=30.

tion using the genetic algorithm.

1. Temperature Effect

The effect of temperature on the $Mn/Na_2WO_4/SiO_2$ catalyst performance in OCM reaction is presented in Fig. 10. Methane conversion, C_2 selectivity and C_2 yield were increased with the increase of temperature (750-850 °C). A temperature increase causes the chemical reaction rates to rise and subsequently an increase methane conversion. This change also causes some heterogeneous reactions overcome gas-phase reactions, and consequently leads to the process advancement. In high temperatures, some consecutive gas-phase reactions developed that operated for yield and selectivity benefit.

2. CH_4/O_2 Ratio Effect

The effect of CH_4/O_2 ratio in the range of 2-6 over the OCM reaction is presented in Fig. 11. It indicates that while CH_4/O_2 ratio was increased in the feed, the selectivity for the C_2 product increased markedly and the conversion of methane and the yield for C_2 product generally decreased too. These results show that higher conversion of methane and C_2 product yield was obtained at higher oxygen ratio (low CH_4/O_2 ratio).

Methane conversion reduction is justified as the following reactions:

$$\text{reaction (4-1):}\quad CH_4+\frac{1}{4}O_2\rightarrow\frac{1}{2}C_2H_6+\frac{1}{2}H_2O\quad E_a\approx 133\frac{Kj}{mol}$$

$$\text{reaction (4-2):}\quad CH_4+\frac{1}{2}O_2\rightarrow\frac{1}{2}C_2H_4+\frac{1}{2}H_2O\quad E_a\approx 350\frac{Kj}{mol}$$

Activation energy of reaction (4-1) was less than reaction (4-2), so the first reaction with less required oxygen occurred very fast. With increase of CH_4/O_2 the amount of C_2H_6 production thereupon increased, whereas C_2H_4 decreased. On the other hand, reaction (4-3) that describes conversion of C_2H_6 to C_2H_4 did not proceed because of lack of sufficient oxygen.

$$\text{reaction (4-3):}\quad C_2H_6+\frac{1}{2}O_2\rightarrow C_2H_4+H_2O$$

Besides, gas-phase reactions which lead to CO_x production (reactions 4-4 and 4-5) dropped substantially.

$$\text{reaction (4-4):}\quad CH_4+\frac{3}{2}O_2\rightarrow CO+2H_2O$$

$$\text{reaction (4-5):}\quad CH_4+2O_2\rightarrow CO_2+2H_2O$$

With considering mentioned changes, C_2 selectivity increased consequently.

The yield of C_2 products was maximized in CH_4/O_2 ratio equal to 4 and then dropped substantially, while selectivity of C_2 products increased continuously.

3. Gas Hourly Space Velocity (GHSV) Effect

The effect of increasing GHSV on the performance of $Mn/Na_2WO_4/SiO_2$ catalyst is presented in Fig. 12. Generally, GHSV increase leads to the reduction of reactant time contact in catalyst bed; therefore, those partial reactions that cause combustion of produced ethane and ethylene do not occur because of time shortage. But, according to Fig. 12, it can be observed that C_2 selectivity has been increased with increase of GHSV from 12,000 to 15,000 $cm^3\ g^{-1}\ h^{-1}$. Afterwards, with increasing of GHSV from 15,000 to 18,000 $cm^3\ g^{-1}\ h^{-1}$, there was a severe drop in selectivity curve and a drastic ascent in conversion curve was observed. The above changes occurred because the temperature of the central section of the catalyst bed was less than the specified amount (850 °C). In these conditions, the furnace starts to work since the central section temperature of the catalyst bed reaches the suitable degree. That is why, by raising the GHSV from 18,000 to 24,000 $cm^3\ g^{-1}\ h^{-1}$, selectivity gradually increases and conversion rate increases with mild slope. The mutual effect of these two parameters causes C_2 yield to increase initially

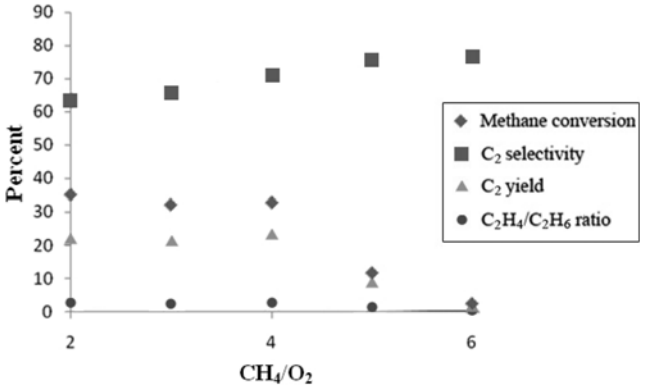

Fig. 11. Effect of CH_4/O_2 ratio over the performance of OCM reaction on $Mn/Na_2WO_4/SiO_2$ catalyst at temperature=850 °C, GHSV=22,464 $cm^3g^{-1}h^{-1}$, mol% N_2=30.

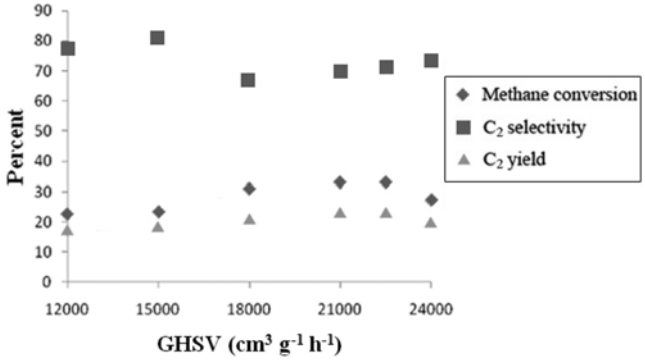

Fig. 12. Effect of GHSV over the performance of OCM reaction on $Mn/Na_2WO_4/SiO_2$ catalyst at temperature=850 °C, CH_4/O_2 ratio=4, mol% N_2=30.

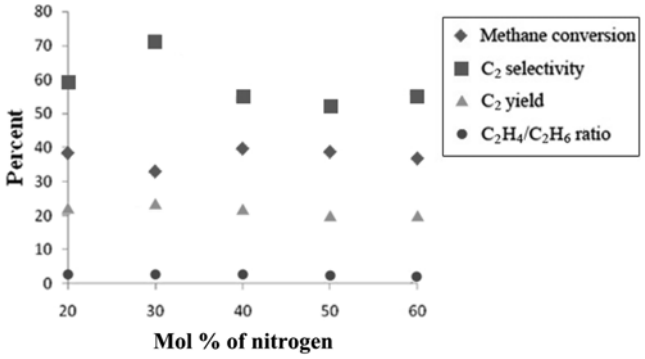

Fig. 13. Effect of mol% N_2 over the performance of OCM reaction on $Mn/Na_2WO_4/SiO_2$ catalyst at temperature=850 °C, GHSV =22,464 $cm^3g^{-1}h^{-1}$, CH_4/O_2 ratio=4.

and then decrease.

4. Diluents Gas Effect

Since the OCM is an extensively exothermic process, one of the important rules of inert gas in this process is temperature control and preventing the formation of hot spots along the reactor. The effect of increasing diluents gas (nitrogen) concentration on the performance of $Mn/Na_2WO_4/SiO_2$ catalyst is shown in Fig. 13. As it is observed, inert gas concentration has an optimum content in this process. Although increase of inert gas concentration leading to decrease of oxygen partial pressure prevents CO_x production, this change is detrimental for OCM reaction.

CONCLUSION

A feed-forward back-propagation network has been developed as a predicting model for OCM process. It was proved that the trained network could well simulate the relations between operation conditions and catalytic performances. The model has been trained, validated and tested on measured data from reactor tests, and then a genetic algorithm has been used to optimize the operating parameters. The obtained results from the experiment under optimum conditions show that the ANN model was able to predict the conversion of methane, C_2 product selectivity, and yield of C_2 and C_2H_4/C_2H_6 ratio with acceptable accuracy. Although using this catalyst under optimum operating conditions did not reach the sufficient yield for industrializing the OCM process, it is suggested to use other different catalysts and perform the experiment in different reactors in further studies to achieve the desirable yield and selectivity.

REFERENCES

1. J. H. Lunsford, *Catal. Today*, **63**, 165 (2000).
2. Y. T. Chua, A. R. Mohamed and S. Bhatia, *Appl. Catal., A*, **343**, 142 (2008).
3. A. Malekzadeh, A. K. Dalai, A. Khodadadi and Y. Mortazavi, *Catal. Commun.*, **9**, 960 (2008).
4. A. Nouralishahi, H. Pahlavanzadeh and J. Towfighi Daryan, *Fuel Process. Technol.*, **89**, 667 (2008).
5. A. Malekzadeh, A. Khodadadi, M. Abedini, M. Amini, A. Bahramian and A. K. Dalali, *Catal. Commun.*, **2**, 241 (2001).
6. S. Mahmoodi, M. R. Ehsani and S. M. Ghoreishi, *J. Ind. Eng. Chem.*, **16**, 923 (2010).
7. D. M. Himmelblau, *Korean J. Chem. Eng.*, **17**(4), 373 (2000).
8. E. A. Medina and J. I. P. Paredes, *Math. Comput. Model.*, **49**, 207 (2009).
9. J. Michalopoulos, S. Papadokonstadakis, G. Arampatzis and A. Lygeros, *Trans. IChemE*, **79**, 137 (2001).
10. J. A. Blasco, N. Fueyo, J. C. Larroya, C. Dopazo and Y. J. Chen, *Comput. Chem. Eng.*, **23**, 1127 (1999).
11. K. L. Priddy and P. E. Keller, *Artificial neural networks: An introduction*, The Soc. of Photo-Opt. Instrum. Eng. (SPIE) Publication, Washington (2005).
12. S. K. Lahiri and K. C. Ghanta, *Chem. Ind. Chem. Eng. Q.*, **15**(2), 103 (2009).
13. E. Barshan, A.Ghodsi, Z. Azimifar and M. Z. Jahromi, *Pattern Recognit.*, **44**, 1357 (2011).
14. I. T. Jolliffe, *Principal component analysis*, 2nd Ed., Springer-Verlag, New York (2002).
15. F. S. Lhabitant, *Hedge funds: Quantitative insights*, John Wily and Sons Ltd., Chichester (2004).
16. K. Deep and K. N. Das, *Appl. Math. Comput.*, **203**, 86 (2008).
17. J. McCall, *J. Comput. Appl. Math.*, **184**, 205 (2005).
18. A. A. Javadi, R. Farmani and T. P. Tan, *Adv. Eng. Inf.*, **19**, 255 (2005).
19. C. C. Wu, P. H. Hsu, J. C. Chen and N. S. Wang, *Comput. Oper. Res.*, **38**, 1025 (2011).
20. G. Corriveau, R. Guilbault and A. Tahan, *Adv. Eng. Softw.*, **41**, 422 (2010).
21. C. J. Huang, Y. J. Chen, C. F. Wu and Y. A. Huang, *Appl. Soft Comput.*, **9**, 824 (2009).
22. J. Cheng, *J. Const. Steel Res.*, **66**, 1011 (2010).
23. L. Jozwiak and A. Postuła, *J. Syst. Archit*, **48**, 99 (2002).